Soil Dynamics and Earthquake Engineering 128 (2020) 105857

Contents lists available at ScienceDirect

Soil Dynamics and Earthquake Engineering

journal homepage: www.elsevier.com/locate/soildyn

Nonlinear system identification on shallow foundation using Extended Kalman Filter

Dong-Kwan Kim[a], Park Hong-Gun[b,**], Dong-Soo Kim[c], Hyerin Lee[d,*]

[a] Dept. of Architectural Engineering, Cheongju University, 298 Daesung-ro, Cheongju, 28503, South Korea
[b] Dept. of Architecture and Architectural Engineering, Seoul National University, 1 Gwanak-ro, Seoul, 08826, South Korea
[c] Dept. of Civil and Environmental Engineering, Korea Advanced Institute of Science and Technology, 291 Daehak-ro, Daejeon, 34141, South Korea
[d] School of Civil and Environmental Engineering, 77 Jeongneung-ro, Seongbuk-gu, Seoul, 02707, South Korea

ARTICLE INFO

Keywords:
Soil-structure interaction
System identification
Shallow foundation
Rocking foundation
Extended kalman filter
Bearing stress

ABSTRACT

This study employs system identification using the Extended Kalman Filter to investigate variations in the stiffness and damping of shallow foundations during earthquakes. System identification results showed that the elastic stiffness of different foundations was significantly smaller than specifications proposed by FEMA 356 for the S_E site class. As the earthquake load increased, a partial uplift of the foundation occurred. Following this uplift, the time domain inelastic stiffness decreased due to variations in contact area between the foundation and sub-soil. The inelastic stiffness at the maximum response was less than the elastic stiffness, according to the effective peak ground acceleration (EPGA) and the contact area ratio. After uplift in the foundation, the EPGA increased, the contact area ratio decreased, and the damping ratio increased by up to 20%. On the basis of these system identification results, we determined relationships between elastic stiffness and the ratio of bearing stress demand to the soil-foundation system capacity.

1. Introduction

The interaction between the soil foundational structure and the rocking effect commonly observed within shallow foundations (which can affect the structural dynamic response) have been investigated since Housner's critical study [1]. To investigate the dynamic behavior of shallow foundations, Antonellis et al. [2] and Madaschi et al. [3] performed full-scale dynamic tests, where Wittich et al. [4], Drosos et al. [5], and Anastasopoulos et al. [6] used small-scale shake table tests.

Recently, experimental studies have used centrifuge tests to investigate rocking effects observed within shallow foundations. For example, these tests were used to study a rocking foundation used as the base isolation for a bridge pier [7], the seismic behavior of a frame-wall-rocking foundation system [8], the structure-soil-structure interaction [9], and rotational damping effects on the structural earthquake response [10].

Numerical studies have been used to predict the dynamic behavior of shallow foundations. For example, Antonellis and Panagiotou [11] compared the seismic response of bridges with unattached rocking foundations to that of fixed-base bridges using numerical analysis. Anastasopoulos and Kontoroupi [12], Chen and Shi [13], and Lu et al. [14] all proposed simplified models to evaluate the seismic response of shallow foundations. Gajan and Kutter [15] used results of centrifuge tests to propose a contact interface model for shallow foundations. These experimental and numerical studies have led to new design concepts that consider shallow foundation rocking effects. This includes studies by Allmond and Kutter [16], who proposed design considerations for rocking foundations that are not connected through piles, Deng et al. [17], who used a displacement-based methodology, and Gazetas et al. [18], who proposed a geotechnical design concept for structures with safety factors that are less than 1.0.

To analyze both test results and the actual rocking shallow foundation, the stiffness of the foundation and sub-soil must be accurately defined. Gazetas [19] proposed impedance functions for the frequency-dependent stiffness and damping of foundation-soil interactions. Deng et al. [20] derived rotational foundation stiffness using centrifuge tests. Most present studies on shallow foundations focus on rotational stiffness, while excluding the effects of translational stiffness. To extract exact properties of soil-foundation structure system, system identification methods have been employed.

System identification is a methodology to analyze parameters of

* Corresponding author.
** Corresponding author.
E-mail addresses: dkkim17@cju.ac.kr (D.-K. Kim), parkhg@snu.ac.kr (H.-G. Park), dskim@kaist.ac.kr (D.-S. Kim), hyerin@kookmin.ac.kr (H. Lee).

https://doi.org/10.1016/j.soildyn.2019.105857
Received 26 March 2018; Received in revised form 17 June 2019; Accepted 6 September 2019
Available online 27 September 2019
0267-7261/

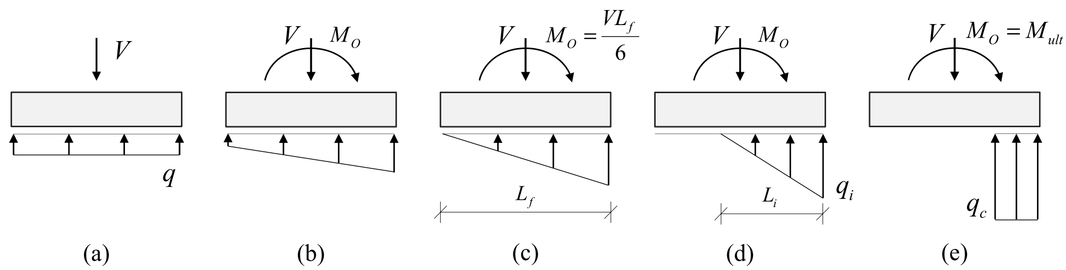

Fig. 1. Variation of stress-bearing distributions according to reaction eccentricity ($q/q_c < 0.5$) [adapted from FEMA 274 [22]]: (a) initial state; (b) elastic state prior to uplift; (c) elastic state at uplift; (d) elastic after uplift; (e) inelastic limit.

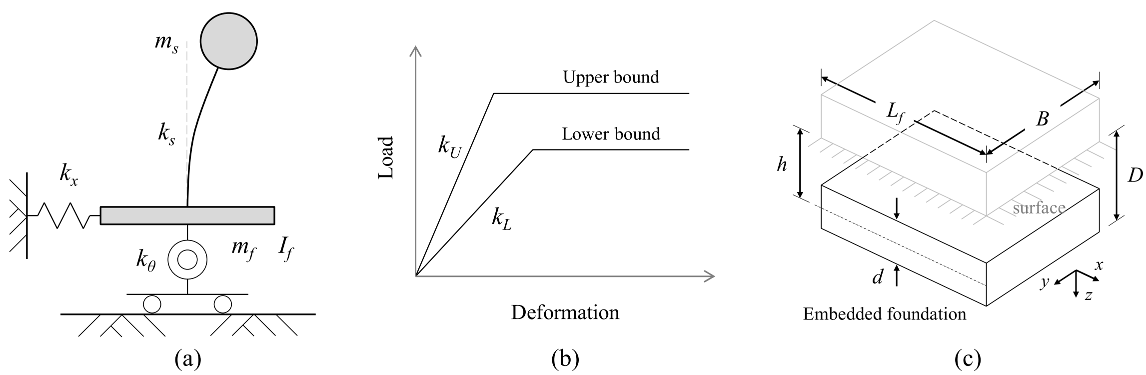

Fig. 2. FEMA 356 considerations [adapted from FEMA 356 (FEMA 2000)]: (a) Uncoupled spring model; (b) Idealized elasto-plastic load deformation behavior; (c) Foundation stiffness properties.

earthquake records and experimental data, based on system model [21]. In the frequency domain, Tilevlioglu et al. [22] proposed dynamic stiffness and shallow foundation damping using the forced vibration of a field test structure. Safak [23] introduced a simple method to convert frequency-dependent impedance functions into time-domain filters and wave propagation method was proposed from actual building data [24]. Also, to supplement the laborious forced vibration test, Ghahari et al. [25] proposed an identification method using free or ambient vibration tests. However, the experimental data of soil and structure by the strong earthquake motion was not enough. Thus, in this study, the centrifuge test [10], which can simulate the soil stress condition and the strong earthquake motion, were used for the system identification. In the time domain, nonlinear system identification using the Extended Kalman Filter could simulate the nonlinear behavior of rocking foundation in Fig. 1.

FEMA 274 [26] shows variations of stress-bearing distribution of the shallow foundation. As the overturning moment increases, uplift occurs at Fig. 1(c). Based on the uplift, decrease of contract area from the elastic state (Fig. 1(b)) to the state after uplift (Fig. 1(d)) affects dynamic responses of the soil-foundation system and the super-structure. Especially, when the uplift occurs, variations of the stiffness and damping should be evaluated in the time domain.

From the nonlinear system identification results, initial elastic stiffness before the uplift (Fig. 1(b)) was evaluated and it was related with the vertical load stress q in Fig. 1(a), which was not accounted in FEMA 356 [27]. After the uplift (Fig. 1(d)), stiffness degradation was quantified according to effective peak ground acceleration (EPGA) and contact area ratio. Also, the increase in damping in Fig. 1(d) due to the mobilization of contact area was evaluated.

2. Existing studies

2.1. FEMA 356

FEMA 356 [24] proposed a flexible base model procedure to address the effects of soil-structure interactions, where an uncoupled spring or Winkler model can also be used. In our study, the uncoupled spring model (as shown in Fig. 1(a), and represented in Eq. (1)) was used to consider the stiffness and damping of shallow foundations.

$$\begin{pmatrix} m_s & m_s & m_s h \\ m_s & m_s + m_f & m_s h \\ m_s h & m_s h & m_s h^2 + I_f \end{pmatrix}\begin{pmatrix} \ddot{u}_{Net} \\ \ddot{u}_{rf} \\ \ddot{u}_\theta \end{pmatrix} + \begin{pmatrix} c_s & 0 & 0 \\ 0 & c_f & 0 \\ 0 & 0 & c_\theta \end{pmatrix}\begin{pmatrix} \dot{u}_{Net} \\ \dot{u}_{rf} \\ \dot{u}_\theta \end{pmatrix} + \begin{pmatrix} k_s & 0 & 0 \\ 0 & k_x & 0 \\ 0 & 0 & k_\theta \end{pmatrix}\begin{pmatrix} u_{Net} \\ u_{rf} \\ u_\theta \end{pmatrix} = -\begin{pmatrix} m_s \\ m_s + m_f \\ m_s h \end{pmatrix}\ddot{u}_g \tag{1}$$

In Eq. (1), u_{Net} is the net lateral displacement of the structure, u_{rf} is the relative displacement between the foundation and sub-soil, u_θ is the foundation rocking angle, h is the vertical distance from the foundation to the lumped structure mass centroid, m_s is the effective structure mass, m_f is the foundation mass, I_f is the foundation's mass moment of inertia, k_s is the structural effective lateral stiffness, and k_x and k_θ are the translational and rotational foundation stiffness. c_s is the structural damping coefficient, and c_x and c_θ are the translational and rotational damping coefficient of foundation.

To use the uncoupled spring model and Eq. (1), FEMA 356 proposed that the translational stiffness $k_{x,surf}$ and rotational stiffness $k_{\theta,surf}$ of the foundation surface be calculated as:

$$k_{x,surf} = \frac{GB}{2-\nu}\left[3.4\left(\frac{L}{B}\right)^{0.65} + 1.2\right] \tag{2}$$

$$k_{\theta,surf} = \frac{GB}{1-\nu}\left[0.47\left(\frac{L}{B}\right)^{2.4} + 0.034\right] \tag{3}$$

where G is the effective shear modulus, ν is Poisson's ratio, and B is the foundation width.

The shear modulus of soil decreases as the shear strain increases. Thus, FEMA 356 defined the effective shear modulus ratio according to the effective peak ground acceleration (EPGA). By using the effective shear modulus ratio r, the effective shear modulus G can be defined as:

Table 1
Effective shear modulus ratio of FEMA 356. To consider the embedment depth effect of the foundation, FEMA 356 proposed correction factors (see Fig. 2(c)).

$$\beta_x = \left(1 + 0.21\sqrt{\frac{D}{B}}\right)\cdot\left[1 + 1.6\left(\frac{hd(B+L)}{BL^2}\right)^{0.4}\right] \tag{5}$$

$$\beta_\theta = 1 + 1.4\left(\frac{d}{L}\right)^{0.6}\left[1.5 + 3.7\left(\frac{d}{L}\right)^{1.9}\left(\frac{d}{D}\right)^{-0.6}\right] \tag{6}$$

Site Class	Effective Shear Modulus Ratio ($r = G/G_0$) Effective peak ground acceleration, $S_{XS}/2.5$			
	$S_{XS}/2.5 = 0$	$S_{XS}/2.5 = 0.1$	$S_{XS}/2.5 = 0.4$	$S_{XS}/2.5 = 0.8$
A	1.00	1.00	1.00	1.00
B	1.00	1.00	0.95	0.90
C	1.00	0.95	0.75	0.60
D	1.00	0.90	0.50	0.10
E	1.00	0.60	0.05	-

$$G = G_0 \cdot r \tag{4}$$

In Eq. (4), $G_0 = V_s^2\rho$, which is the initial shear modulus, V_s is the shear wave velocity of soil, ρ is the soil mass density, and r is the effective shear modulus ratio (shown in Table 1). In this study, the shear modulus reduction was considered when stiffness was calculated, but the variations in stress between the foundation and sub-soil (shown in Fig. 1(b–d)) were not.

In these equations, d is the height of the effective side-wall contact and h is the depth from the ground surface to the centroid of effective side wall contact. Foundation geometry details are presented in Fig. 2(c).

The elastic stiffness of foundation can be redefined by multiplying correction factors related to embedment as:

$$k_x = k_{x,sur} \cdot \beta_x \tag{7}$$

$$k_\theta = k_{\theta,suff} \cdot \beta_\theta \tag{8}$$

When a shallow foundation is subjected to overturning force, variations in the bearing stress distribution (according to eccentricities with in the foundation's reaction) can be represented as in Fig. 1. Fig. 1(a) shows the uniform bearing stress value q without the overturning moment M_o. When a large overturning moment is applied, the ultimate bearing capacity of the foundation can be estimated using the uniform stress block, as shown in Fig. 1(e). The ultimate moment capacity M_{ult} of a rectangular foundation (Fig. 1(e)) can be calculated according to FEMA 356:

$$M_{ult} = \frac{V \cdot L_f}{2} \cdot \left(1 - \frac{q}{q_c}\right) \tag{9}$$

where V is the axial load acting on the foundation, L_f is the foundation length, and q_c is the ultimate bearing capacity of the soil. In Eq. (9), the q/q_c ratio of bearing stress demand to capacity affects the ultimate moment capacity M_{ult}. Thus, the ultimate moment capacity M_{ult} varies from lower to upper bounds (according to the bearing stress ratio), as shown in Fig. 2(b). Also, the q/q_c ratio can be an index to indicate the vertical bearing stress level of the structure-foundation system.

When the overturning moment reaches one-sixth of the $V \cdot L_f$, a partial uplift occurs between the foundation and sub-soil. Thus, the bearing stress distribution in Fig. 1(c) can be considered the linear limit state. When the q/q_c ratio is smaller than 0.5, the bearing stress linearly distributes with the reduced contact area L_i and the stress q_i shown in Fig. 1(d) (FEMA 274). Thus, the overturning moment levels varied from the elastic state (Fig. 1(b)) to the inelastic limit state (Fig. 1(e)). When the soil stress distribution was in the inelastic limit state (Fig. 1(e)), the extreme contact area moved from one side to the other under cyclic loading, and the stiffness was significantly degraded. Therefore, the stiffness and damping of the foundation were not accurately estimated. Because of this, test results shown in Fig. 1(d) were used to estimate the foundation's stiffness and damping. The state of Fig. 1(d) indicates that the contact area is reduced and the material is in elastic state.

2.2. Centrifuge test on the soil-foundation-structure system

Centrifuge tests were performed to investigate how the rocking effect changes the way structures respond to earthquakes [10]. Centrifuge tests were performed using 20 g of centrifugal acceleration. Two structures with periods of 0.26 s and 0.36 s, which were measured with the fixed base condition, were used. The dimensions of test structures used are presented in Fig. 3(b–c) (see Fig. 4).

For centrifuge tests, the external dimensions of the foundation were 70 × 70 × 30 mm in the small-scale model, which was tested under 20 g of centrifugal acceleration. Thus, the prototype model's external foundation dimensions were 1.4 × 1.4 × 0.6 m. Table 2 summarizes soil and foundation properties applicable for centrifuge tests [10]. S_E was used as a site class for the centrifuge tests, where the soil bearing stress to strength ratio q/q_c was 0.016 for SDOF-3 and 0.021 for SDOF-4. These parameters indicate that the soil was not stiff, and the axial compression at the foundation was thus small (see Table 3).

The nyquist frequency of measurements was 100 Hz. The measured horizontal accelerations of the structure and the foundation ($\ddot{u}_t$ and, $\ddot{u}_f$ in Fig. 3) and the two vertical accelerations at the edges of the foundation ($\ddot{u}_{v1}$ and, $\ddot{u}_{v2}$ in Fig. 3) were converted to displacements using the

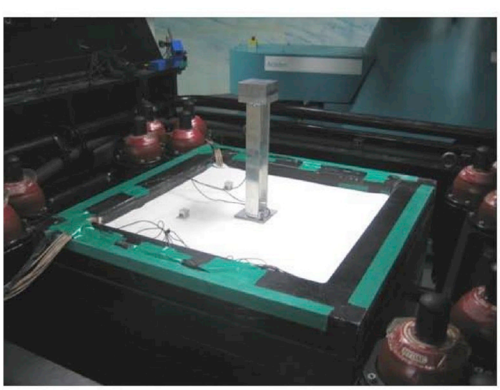
(a) Test specimen (20 g centrifugal acceleration)

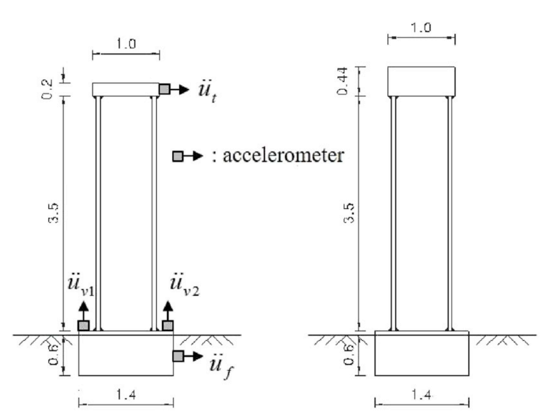

(b) SDOF-3
$T_n = 0.26$ s / $q/q_c = 0.016$

(c) SDOF-4
$T_n = 0.36$ s / $q/q_c = 0.021$

Fig. 3. Centrifuge tests for system identification (Kim et al., 2015).

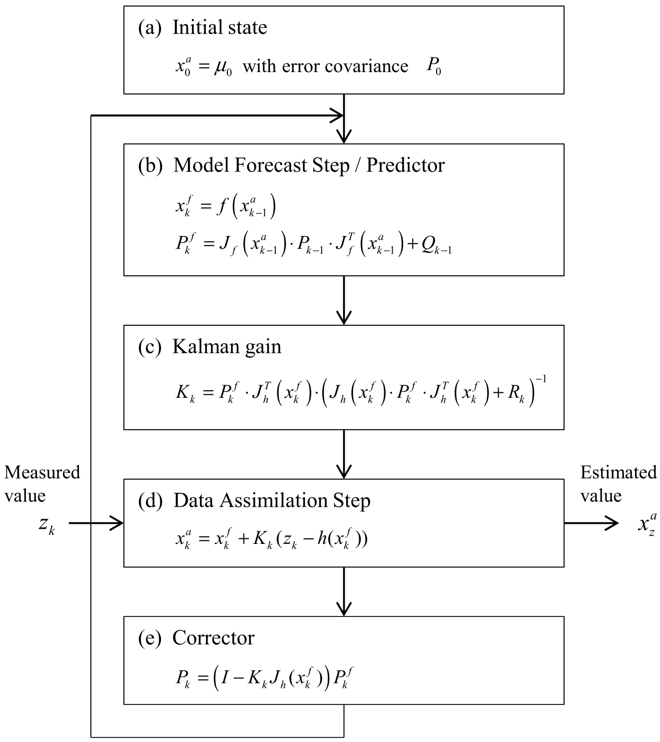

Fig. 4. Extended Kalman Filter algorithm.

double integration method. A high-pass filter was used to prevent the divergence of the integration of the measured acceleration. The cut-off frequencies were determined as follows.

$$\ddot{u}_t = \frac{-c_s(\dot{u}_t - \dot{u}_f - h \cdot \dot{u}_\theta) - k_s(u_t - u_f - h \cdot u_\theta)}{m_s} \tag{10}$$

where $u_f = u_g + u_{rf}$, $u_t = u_f + u_\theta h + u_{Net}$, and $u_\theta = (u_{v1} - u_{v2})/L_f$

In Eq. (10), $\ddot{u}_t$ indicates the measured total acceleration of the structure, and the right side of Eq. (10) is the acceleration calculated from the velocities and displacements that are integrated from the filtered accelerations. Using Eq. (10), the cut-off frequency, which produced the same value for the left side and right side, was determined. The cut-off frequency was found by trial and error [10].

From the test result, the vertical displacement u_v of the soil-foundation system was calculated as $u_v = (u_{v1} + u_{v2})/2$. Because the vertical displacement was very small, it was not considered in this study.

3. Nonlinear system identification using an Extended Kalman filter

3.1. Extended Kalman Filter

To estimate stiffness (k_x and k_θ) and damping (c_x and c_θ) for the soil-foundation system from test results (as shown in Eq. (1)), we used the Extended Kalman Filter. The Extended Kalman Filter estimates unknown values on the basis of both measured values and the system function. We used an Extended Kalman Filter algorithm as per Terejanu [28] and Kim [29].

Table 3
FEMA 356 foundation stiffness.

Initial stiffness of foundation at the surface		Embedment correction factor		Initial stiffness of embedded foundation	
$k_{x,surf}$ (kN/m)	$k_{\theta,surf}$ (kN·m/rad)	β_x	β_θ	k_{x0} (kN/m)	$k_{\theta 0}$ (kN·m/rad)
151,116	78,812	2.06	2.89	311,525	227,446

3.2. State space expressions of the SSI model

To use the Extended Kalman Filter, the process function $f(\cdot)$ should be a forward process. Thus, Eq. (1) was expressed in a state-space according to Mikami and Sawada [30], and was modified for the centrifuge test results. To obtain a state-space expression, Eq. (1) can be expressed in a simple form as:

$$[M]\{\ddot{U}(t)\} + [C]\{\dot{U}(t)\} + [K]\{U(t)\} = \{F(t)\} \tag{11}$$

By solving Eq. (11) using a linear acceleration method, the following equations can be obtained:

$$\{Z_1(k+1)\} = [A]^{-1}[\{F(k+1)\} - [C]\{a(k)\} - [K]\{b(k)\}] \tag{12}$$

$$\{Z_2(k+1)\} = \{a(k)\} + \frac{1}{2}\Delta t\{Z_1(k+1)\} \tag{13}$$

$$\{Z_3(k+1)\} = \{b(k)\} + \frac{1}{6}\Delta t^2\{Z_1(k+1)\} \tag{14}$$

where:

$$[A] = [M] + \frac{1}{2}\Delta t[C] + \frac{1}{6}\Delta t^2[K] \tag{15}$$

$$\{a(k)\} = \{\dot{u}(k)\} + \frac{1}{2}\Delta t\{\ddot{u}(k)\} \tag{16}$$

$$\{b(k)\} = \{u(k)\} + \Delta t\{\dot{u}(k)\} + \frac{1}{3}\Delta t^2\{\ddot{u}(k)\} \tag{17}$$

$$F(k+1) = -\begin{Bmatrix} m_s \\ m_s + m_f \\ m_s H \end{Bmatrix}\ddot{u}_g(k+1) \tag{18}$$

In the above equations, k is the time step, Δt is the time increment, and the time at time step k is expressed as $t_k = k\Delta t$. $\{\ddot{U}(k)\}$, $\{\dot{U}(k)\}$, $\{U(k)\}$ are expressed via the state vectors $\{Z_1(k)\}$, $\{Z_2(k)\}$, $\{Z_3(k)\}$.

These equations express the forward process from time step k to $k+1$, except for the input term $F(k+1)$. The input term $F(k+1)$ includes the ground acceleration factor $\ddot{u}_g(k)$, where the ground acceleration difference $w(k)$ can be expressed as:

$$w(k) = \ddot{u}_g(k+1) - \ddot{u}_g(k). \tag{19}$$

Using the ground acceleration difference, the transition of the input acceleration, velocity, and displacement can be expressed as:

$$\{Z_6(k+1)\} = [B]\{Z_6(k)\} + [D]w(k) \tag{20}$$

Table 2
Soil and foundation properties (Kim et al., 2015).

Soil			Foundation				
Centrifugal acceleration	Average shear wave velocity	Initial shear Modulus (G_0)	Length (L)	Width (B)	D	d	h
20 g	162 m/s	39.9 MPa	1.4 m	1.4 m	0.6 m	0.6 m	0.3 m

where:

$$\{Z_6(k)\} = \begin{Bmatrix} \ddot{u}_g(k) \\ \dot{u}_g(k) \\ u_g(k) \end{Bmatrix} \tag{21}$$

$$[B] = \begin{bmatrix} 1 & 0 & 0 \\ \Delta t & 1 & 0 \\ \Delta t^2/2 & \Delta t & 1 \end{bmatrix} \tag{22}$$

$$[D] = \begin{Bmatrix} 1 \\ \Delta t/2 \\ \Delta t^2/6 \end{Bmatrix}. \tag{23}$$

From Eq. (18), the input term *F(k+1)* is expressed as:

$$\{F(k+1)\} = [E]\{Z_6(k+1)\} \tag{24}$$

where:

$$[E] = \begin{bmatrix} -m_s & 0 & 0 \\ -(m_s+m_f) & 0 & 0 \\ -m_s H & 0 & 0 \end{bmatrix}. \tag{25}$$

By substituting Eq. (20) into Eq. (24), Eq. (26) can be obtained as:

$$\{F(k+1)\} = [E][B]\{Z_6(k)\} + [E]\{D\}w(k). \tag{26}$$

with this manipulation, equations (12)–(14) become a purely forwarding process from time step k to $k+1$.

Both the structure mass and the foundation's mass moment of inertia are known from the centrifuge tests. Thus, by inserting values for stiffness k_x, k_f, and k_θ into the state vector $\{Z_4\}$, and values for damping coefficients c_x, c_f, and c_θ into the state vector $\{Z_5\}$, vector transitions can be expressed as:

$$\{Z_4(k+1)\} = \{Z_4(k)\} \tag{27}$$

$$\{Z_5(k+1)\} = \{Z_5(k)\}. \tag{28}$$

By taking into account the accelerations, velocities, and displacements at each degree of freedom at the base, the following state-space expression is obtained:

$$\{Z(k+1)\} = G\{Z(k)\} + \{\Gamma(k)\}w(k) \tag{29}$$

where $\{Z\}$ and $G\{Z\}$ are composed of multiple vectors, which can be expressed as:

$$\{Z\} = [\{Z_1\}^T,\ \{Z_2\}^T,\ \{Z_3\}^T,\ \{Z_4\}^T,\ \{Z_5\}^T,\ \{Z_6\}^T] \tag{30}$$

$$G\{Z(t)\} = [\{G_1\}^T,\ \{G_2\}^T,\ \{G_3\}^T,\ \{G_4\}^T,\ \{G_5\}^T,\ \{G_6\}^T] \tag{31}$$

where:

$$G_1 = [A]^{-1}\{[E][B]\{Z_6\} - [C]\{a\} - [K]\{b\}\} \tag{32}$$

$$G_2 = \{a\} + \frac{1}{2}\Delta t \cdot G_1 \tag{33}$$

$$G_3 = \{b\} + \frac{1}{6}\Delta t^2 \cdot G_1 \tag{34}$$

$$G_4 = \{Z_4\} \tag{35}$$

$$G_5 = \{Z_5\} \tag{36}$$

$$G_6 = B\{Z_6\} \tag{37}$$

$$\{\Gamma(k)\} = \begin{Bmatrix} [A]^{-1}[E]\{D\} \\ \Delta t[A]^{-1}[E]\{D\}/2 \\ \Delta t^2[A]^{-1}[E]\{D\}/6 \\ 0 \\ 0 \\ \{D\} \end{Bmatrix}. \tag{38}$$

3.3. Linearization of state equation

The Kalman Filter was originally developed to identify linear systems. As mentioned previously, the Extended Kalman Filter can be used to identify nonlinear systems by assuming that nonlinear behavior can be approximated as a linear system with small perturbations [30].

By assuming that $G\{Z(k)\}$ is a smooth function, the Taylor expansion of $G\{Z(k)\}$ can be used to estimate the optimal time step k, where the truncated form of $G\{Z(k)\}$ can be obtained by ignoring terms of the Taylor expansion higher than the second order. Thus, Eq. (29) can be expressed as:

$$\{Z(k+1)\} = G\{\hat{Z}(k|k)\} + \Phi(k+1|k)\{Z(k) - \hat{Z}(k|k)\} + \{\Gamma(k)\}w(k) \tag{39}$$

where $\Phi(k+1|k)$ is a transition matrix, which is expressed as:

$$\Phi(k+1|k) = \left[\frac{\partial G\{Z(k)\}}{\partial Z_j}\right]_{Z(k)=Z(k|k)} \quad (j = 1, \ldots, 18) \tag{40}$$

where the components are computed as:

$$\frac{\partial G_1}{\partial Z_j} = [A]^{-1}\left(-\frac{\partial [A]}{\partial Z_j}G_1 + [E][B]\frac{\partial \{Z_6\}}{\partial Z_j} - \frac{\partial [C]}{\partial Z_j}\{a\} - [C]\frac{\partial \{a\}}{\partial Z_j}\right) + [A]^{-1}\left(-\frac{\partial [K]}{\partial Z_j}\{b\} - [K]\frac{\partial \{b\}}{\partial Z_j}\right) \tag{41}$$

$$\frac{\partial G_2}{\partial Z_j} = \frac{\partial \{a\}}{\partial \{Z_j\}} + \frac{1}{2}\Delta t\frac{\partial G_1}{\partial Z_j} \tag{42}$$

$$\frac{\partial G_3}{\partial Z_j} = \frac{\partial \{b\}}{\partial \{Z_j\}} + \frac{1}{6}\Delta t^2\frac{\partial G_1}{\partial Z_j} \tag{43}$$

$$\frac{\partial G_4}{\partial Z_j} = \begin{bmatrix} 0 & \cdots & 0 & 1 & 0 & 0 & 0 & 0 & 0 & 0 & 0 & 0 \\ 0 & \cdots & 0 & 0 & 1 & 0 & 0 & 0 & 0 & 0 & 0 & 0 \\ 0 & \cdots & 0 & 0 & 0 & 1 & 0 & 0 & 0 & 0 & 0 & 0 \end{bmatrix}_{3\times 18} \tag{44}$$

$$\frac{\partial G_5}{\partial Z_j} = \begin{bmatrix} 0 & \cdots & 0 & 1 & 0 & 0 & 0 & 0 & 0 \\ 0 & \cdots & 0 & 0 & 1 & 0 & 0 & 0 & 0 \\ 0 & \cdots & 0 & 0 & 0 & 1 & 0 & 0 & 0 \end{bmatrix}_{3\times 18} \tag{45}$$

$$\frac{\partial G_6}{\partial Z_j} = \begin{bmatrix} 0 & \cdots & 0 & 1 & 0 & 0 \\ 0 & \cdots & 0 & \Delta t & 1 & 0 \\ 0 & \cdots & 0 & \Delta t^2/2 & \Delta t & 1 \end{bmatrix}_{3\times 18}. \tag{46}$$

3.4. Observation equation

The accelerations of the structure, foundation, and soil were measured using centrifuge tests. Velocities and displacements of the structure, foundation, and soil were calculated from measured acceleration using the high-pass filter and double integration method [10]. Structural stiffness and damping were also estimated from the properties of the test specimen, where the observation equation was:

$$\{Y(k)\} = [H]\{U(k)\} + \{v(k)\} \tag{47}$$

where $[H]$ is the observation matrix, and is expressed as:

$$[H] = \begin{bmatrix} 1&0&0&0&0&0&0&0&0&0&0&0&0&0&0&0&0&0\\ 0&1&0&0&0&0&0&0&0&0&0&0&0&0&0&0&0&0\\ 0&0&1&0&0&0&0&0&0&0&0&0&0&0&0&0&0&0\\ 0&0&0&1&0&0&0&0&0&0&0&0&0&0&0&0&0&0\\ 0&0&0&0&1&0&0&0&0&0&0&0&0&0&0&0&0&0\\ 0&0&0&0&0&1&0&0&0&0&0&0&0&0&0&0&0&0\\ 0&0&0&0&0&0&1&0&0&0&0&0&0&0&0&0&0&0\\ 0&0&0&0&0&0&0&1&0&0&0&0&0&0&0&0&0&0\\ 0&0&0&0&0&0&0&0&1&0&0&0&0&0&0&0&0&0\\ 0&0&0&0&0&0&0&0&0&1&0&0&0&0&0&0&0&0\\ 0&0&0&0&0&0&0&0&0&0&0&0&1&0&0&0&0&0\\ 0&0&0&0&0&0&0&0&0&0&0&0&0&0&0&1&0&0\\ 0&0&0&0&0&0&0&0&0&0&0&0&0&0&0&0&1&0\\ 0&0&0&0&0&0&0&0&0&0&0&0&0&0&0&0&0&1 \end{bmatrix}_{14\times 18} \quad (48)$$

In this equation, $\{v(k)\}$ is the observation noise vector, which is assumed to have the following characteristics:

$$E[\{Y(k)\}] = \{0\} \quad (49)$$

$$E[\{v(k)\}\cdot\{v(k)\}^T] = [R(t)] \quad (50)$$

where $[R(t)]$ is the observation noise covariance matrix.

4. Comparing test and system identification results

4.1. Estimated stiffness and damping coefficients

Fig. 5 and Fig. 7 show nonlinear stiffness and damping coefficients, which were estimated via system identification using the Extended Kalman Filter. We used the Northridge earthquake for input earthquake acceleration (Fig. 5), and an effective peak ground acceleration (EPGA) at surface of 0.257 g. The EPGA of the ground motions were calculated by dividing the average spectral acceleration of the period range of 0.1–0.5 s by a factor of 2.5, according to ATC 3-06 [31]. The corresponding FEMA 356 effective shear modulus ratio was 0.31 derived from Table 1, and the q/q_c ratio was 0.016.

Fig. 5(a) shows variations in both the translational stiffness($k_{x,SI}$) and the damping coefficient($c_{x,SI}$) in the time domain. After partial uplift of the foundation (shown in Fig. 1(c)), the translational stiffness rapidly decreased, due to the decrease in contact area between the foundation and the sub-soil. During this time, the translational damping also increased, as shown in Figs. 5(a-2). The stiffness at the onset of uplift is considered to be elastic, where the initial stiffness($k_{x,SI}$ = 36981 kN/m) estimated by system identification was significantly smaller than the translational stiffness calculated using FEMA 356 ($k_{x,FEMA}$ = 0.31 k_{x0} = 97213 kN/m), which also decreased upon a reduction in shear modulus *r*. After the initial uplift, the contact area distribution changed to the elastic after uplift state (as shown in Fig. 1(d)), in which the stiffness was reduced from 36,981 to 19,610 kN/m. Furthermore, mobilization of the contact area between the foundation and the sub-soil increased the damping coefficient from 19.4 to 76.1 kN s/m. The corresponding damping ratios increased from 0.035 to 0.188, which was calculated as:

$$\xi_x(t) = c_x(t)/2\sqrt{k_x(t)\cdot m_f}. \quad (51)$$

Fig. 5(b) shows variations in the rotational stiffness ($k_{\theta,SI}$) and damping coefficient ($c_{\theta,SI}$) in the time domain. For the Extended Kalman Filter, 30,000 kN m/rad was used as the assumed initial rotational stiffness. As the earthquake started, the Extended Kalman Filter increased the elastic stiffness to 41,466 kN m/rad to find the correct stiffness from the assumed stiffness. After this uplift, the estimated rotational stiffness decreased from 41,466 to 24,070 kN m/rad, which was significantly smaller than that derived from FEMA 356 ($k_{\theta,FEMA}$ = 0.31 $k_{\theta 0}$ = 70,975 kN m/rad). The rotational damping coefficient increased from 89.8 kN·m·s/rad to 300.5 kN m·s/rad; the corresponding damping ratios increased from 0.036 to 0.163, and were calculated as:

$$\xi_\theta(t) = c_\theta(t)/2\sqrt{k_\theta(t)\cdot(m_s h^2 + I_f)}. \quad (52)$$

It is notable that the stiffness after the maximum displacement and rotation did not change significantly, even though the ground excitation gradually disappeared (as shown in Fig. 6). Additionally, damping coefficients after the maximum displacement and rotation gradually increased. This indicates that the system identification used in this study simulated the decrease of foundation response by controlling the damping increase, rather than restoring the stiffness. Thus, the stiffness at the maximum response was considered as the maximum inelastic stiffness.

Fig. 7 shows the results of SDOF-4. The input earthquake acceleration was that of the Northridge earthquake and the effective peak ground acceleration (EPGA) at surface was 0.274 g. The corresponding effective shear modulus ratio derived from Table 1 was 0.28. As the EPGA of Fig. 7 (0.274 g) was greater than the EPGA of Fig. 5 (0.257 g), the effective shear modulus ratio(0.28) and corresponding stiffness of FEMA 356 in Fig. 7 ($k_{x,FEMA}$ = $0.28k_{x0}$ = 87,167 kN/m, $k_{\theta,FEMA}$ = $0.28k_{\theta 0}$ = 63,641 kN m/rad) were smaller than the effective shear

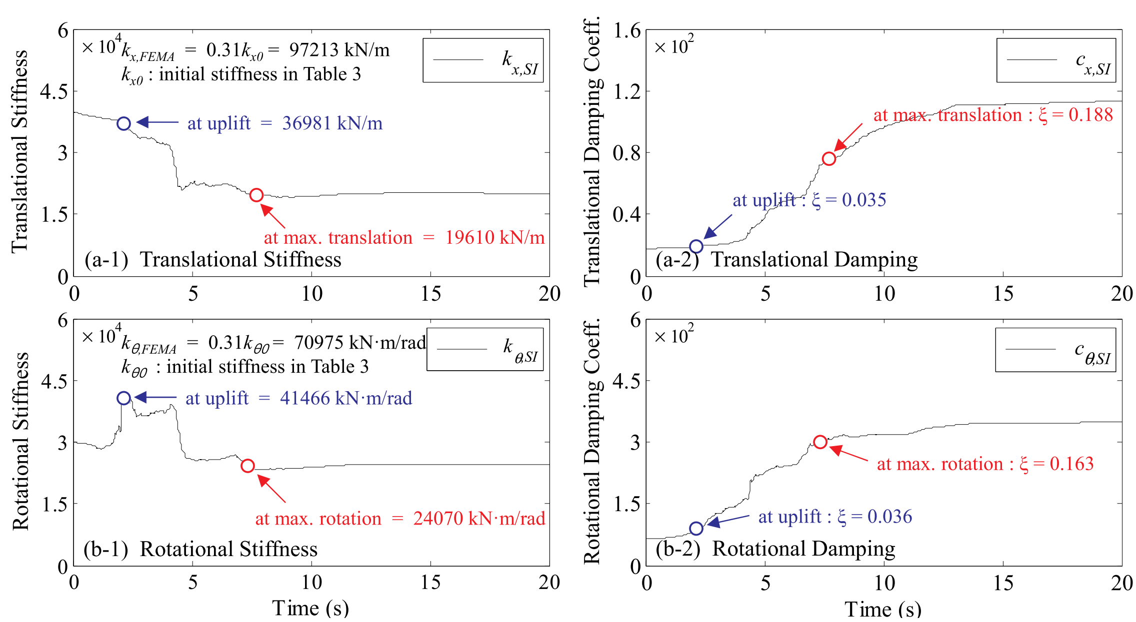

Fig. 5. Estimated stiffness and damping coefficients: SDOF-3 (q/q_c = 0.016); EPGA at input base = 0.092 g; EPGA at surface = 0.257 g.

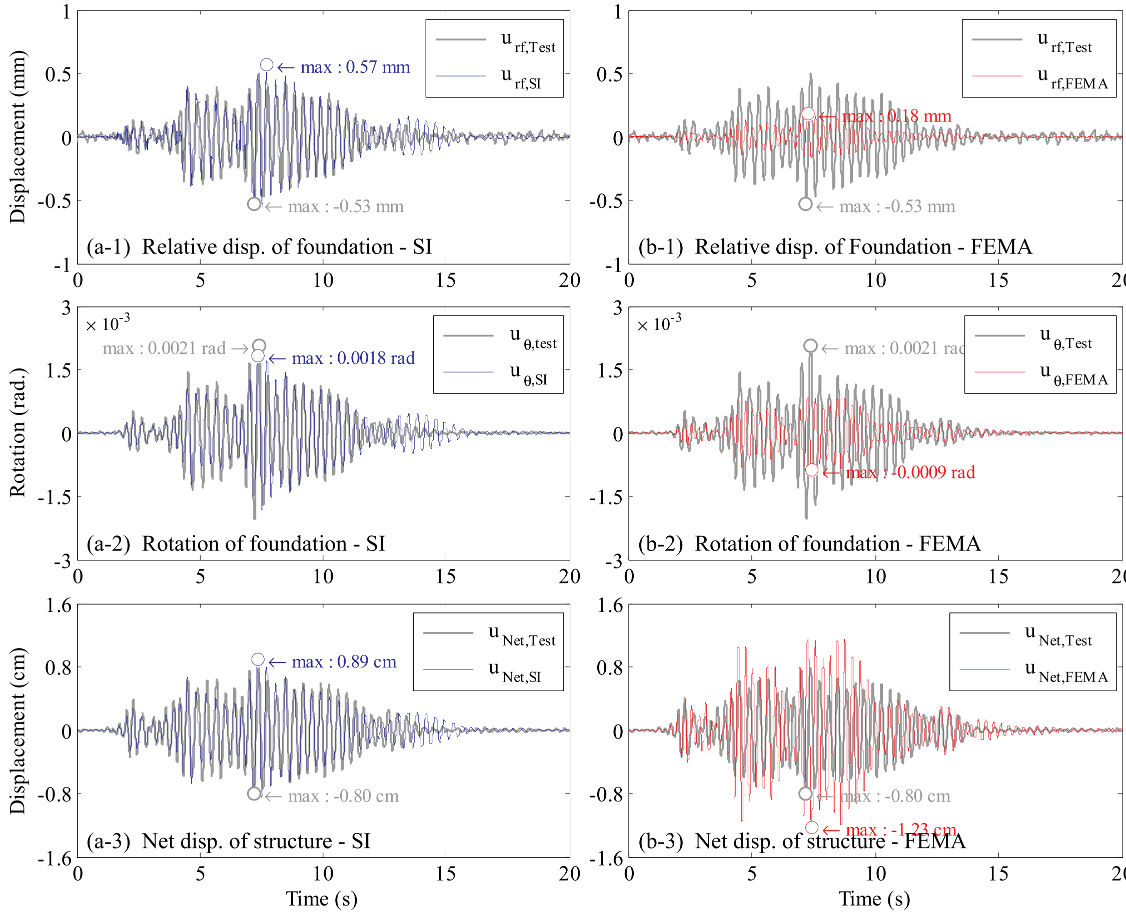

Fig. 6. Time history response for both the foundation and the structure: SDOF-3 (T_n = 0.26 s); EPGA at input base = 0.092 g; EPGA at surface = 0.257 g.

modulus ratio (0.31) and corresponding stiffness of FEMA 356 in Fig. 5 ($k_{x,FEMA}$ = 0.31 k_{x0} = 97,213 kN/m, $k_{\theta,FEMA}$ = 0.31 $k_{\theta 0}$ = 70,975 kN m/rad). However, the estimated initial elastic translational and rotational stiffness in Fig. 7 ($k_{x,SI}$ = 47,041 kN/m, $k_{\theta,SI}$ = 53,723 kN m/rad) were greater than those shown in Fig. 5($k_{x,SI}$ = 36,981 kN/m, $k_{\theta,SI}$ = 41,466 kN m/rad). This is because the q/q_c of SDOF-4 in Fig. 7 was 30% greater than the q/q_c of SDOF-3 shown in Fig. 5.

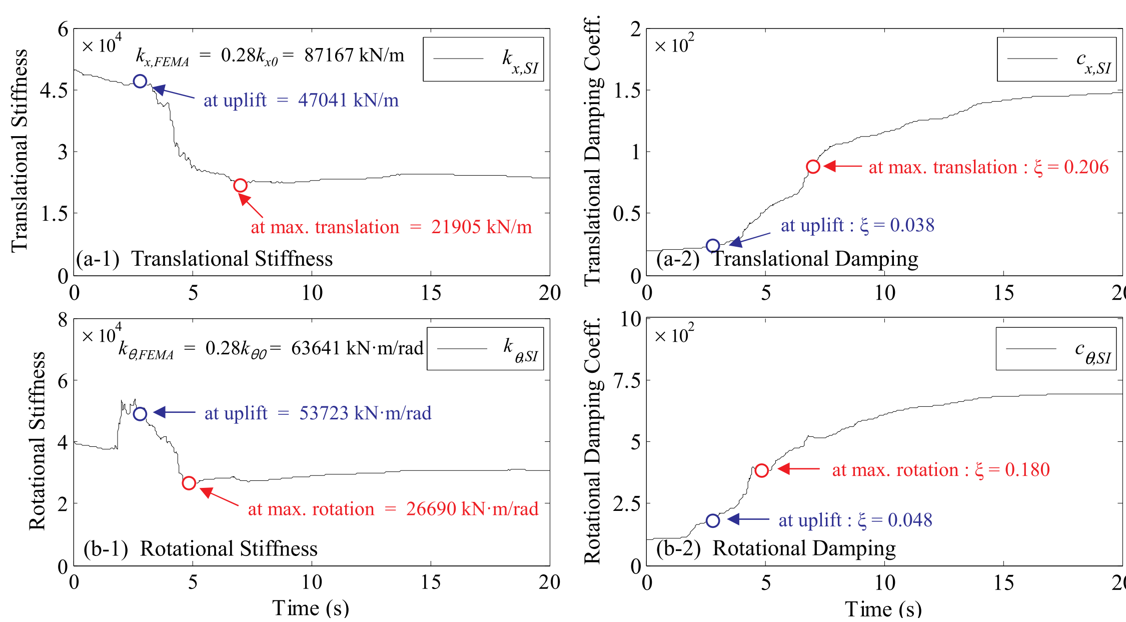

Fig. 7. Estimated stiffness and damping coefficients: SDOF-4 (q/q_c = 0.021); EPGA at input base = 0.108 g; EPGA at surface = 0.274 g.

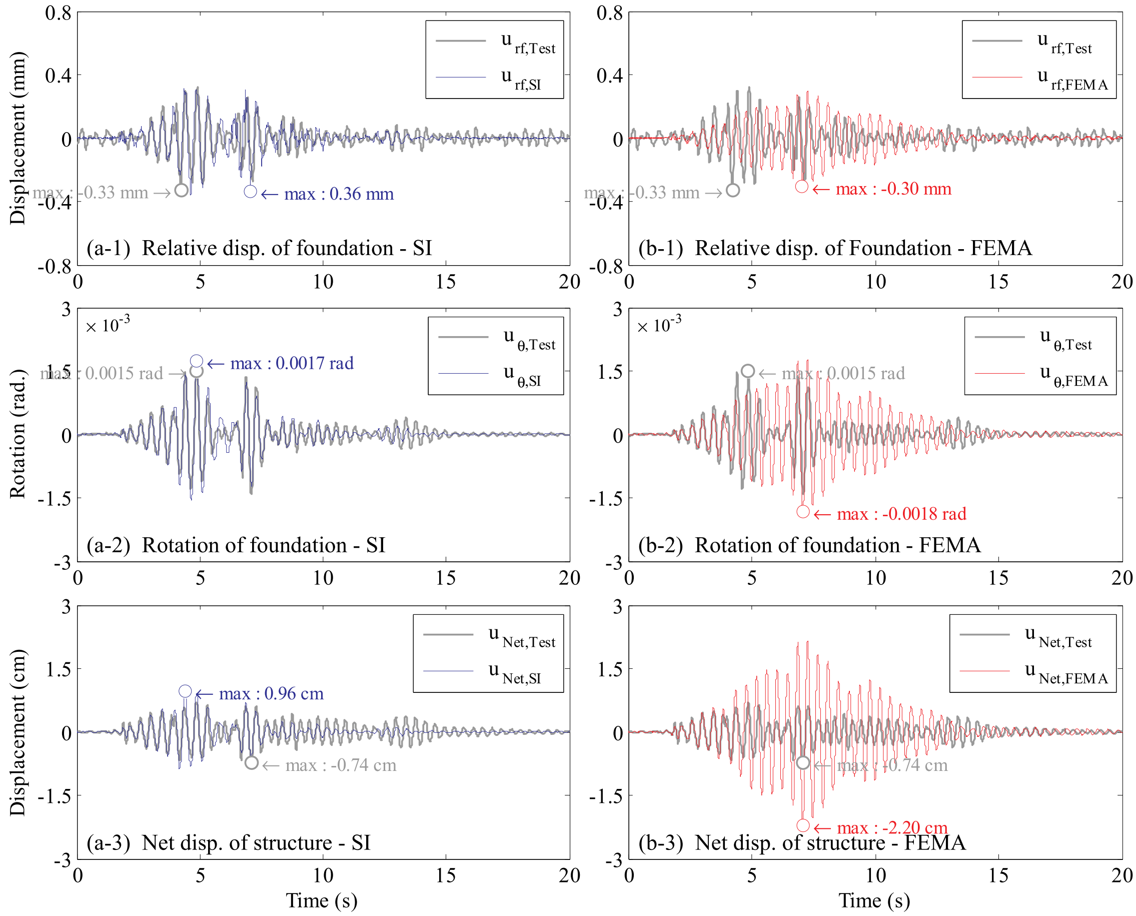

Fig. 8. Time history responses for both the foundation and the structure: SDOF-4 (T_n = 0.36 s); EPGA at input base = 0.108 g; EPGA at surface = 0.274 g.

4.2. Foundation and structure time history responses

The time history response of the foundation and structure was calculated by applying the estimated stiffness and damping coefficients to Eq. (1), where Figs. 6 and Fig. 8 show the relative translational displacement of the foundation u_{rf}, the rotation angle of the foundation u_θ, and the net displacement of the structure u_{net}. In comparison, time history responses of the foundation and the structure were calculated using the FEMA 356 stiffness and 5% damping ratios.

As the FEMA 356 stiffness was 1.71 and 2.63 times the estimated stiffness shown in Figs. 5(a-1) and Fig. 5(b-1), both the FEMA 356 translational relative displacement and the rotational angle were smaller than the test results shown in Figs. 6(b-1) and Fig. 6(b-2).On the other hand, the translational relative displacement and the rotational angle calculated using stiffness and damping estimated from system identification correlated well with the test results, in terms of both peaks and shape of the time history response, as shown in Figs. 6(a-1) and Fig. 6(a-2).

Figs. 6(a-3) and Fig. 6(b-3) show the net displacement of the structure. The maximum net displacement of the test was 0.80 cm (Figs. 6(b-3)). FEMA 356 underestimated the translational and rotational response of the foundation, where the net displacement of the structure was greater than within our test results. On the other hand, the net displacement of the structure using stiffness and damping estimated using system identification coincided well with the test results (shown in Figs. 6(a-3)).

For SDOF-4 (with a period of 0.36s), the shapes and peaks of the foundation response (calculated using the FEMA 356 stiffness and a 5% damping ratio) did not agree with our test results (Figs. 7(b-1)-7(b-3)). The net displacement of structure from the centrifuge test were affected by the energy dissipation and the increase in damping due to the mobilization of contact area. However, FEMA 356 estimated the response of structure with the fixed stiffness and damping of foundation. Thus, the net displacement of the structure was overestimated by FEMA 356 in Figs. 8(b-3). Alternatively, time history responses (calculated using the stiffness and damping coefficients estimated from system identification) were very close to the test results (Figs. 7(a-1)-7(a-3)). This indicates that the estimated stiffness and damping coefficients are reasonable.

4.3. Relationship between elastic stiffness and bearing stress

FEMA 356 stiffness, and elastic stiffness estimated by SI are presented in Fig. 8(a), (b) and Fig. 9(a), (b). EPGA at surface varied from 0.1 to 0.3 g, where the FEMA 356 translational and rotational stiffness were reduced from 0.60 k_{x0} and 0.60 $k_{\theta0}$ to 0.23 k_{x0} and 0.23 $k_{\theta0}$, respectively, due to the reduction in sub-soil shear modulus.

However, the black-circle makers in Fig. 8(a), (b) and Fig. 9(a), (b), which were considered as the elastic stiffness of foundation before the partial uplift in Fig. 1(b), was significantly smaller than that from FEMA 356. Also, when EPGA varies from 0.1 to 0.3 g, variations of the elastic stiffness according to the EPGA was small.

When the q/q_c ratio, which was the normalized vertical bearing stress q by the ultimate bearing capacity q_c, was 0.016 (as for SDOF-3), the mean elastic translational stiffness was 0.12 k_{x0} and the mean elastic rotational stiffness was 0.19 $k_{\theta0}$, as shown in Figs. 8(a-2) and 8(b-2). When the q/q_c ratio was 0.021 (as for SDOF-4), the mean elastic translational stiffness was 0.15 k_{x0} and the mean elastic rotational stiffness was 0.25 $k_{\theta0}$, as shown in Figs. 8(a-2) and 9(a-2). As the q/q_c ratios increased from 0.016 to 0.021, the translational and rotational

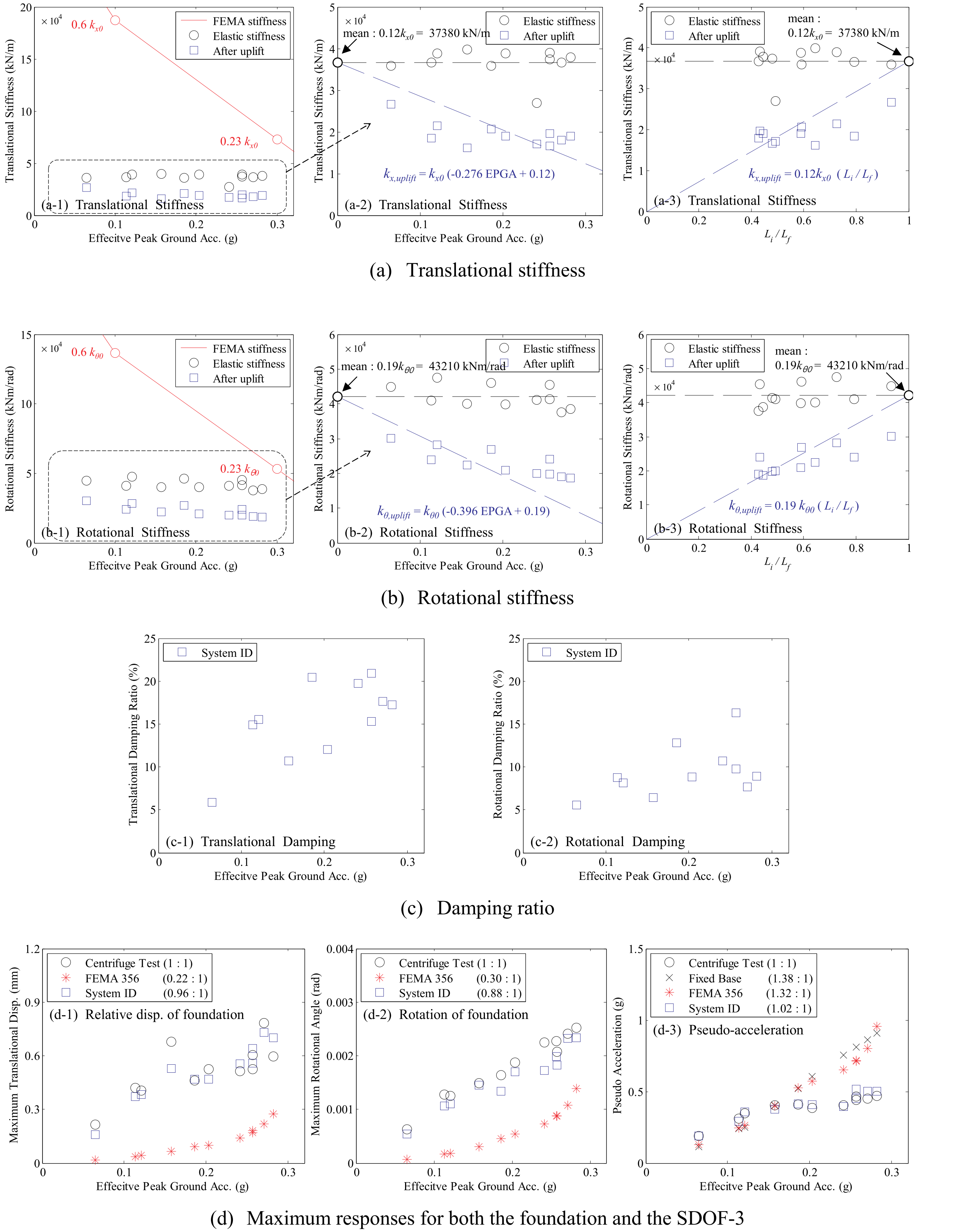

Fig. 9. System identification results for SDOF-3.

stiffness in the elastic state were increased. This indicates that the vertical bearing stress affects the stiffness of shallow foundation.

By using both the stiffness of FEMA 356 and the system identification results, relationships between the elastic stiffness and the bearing stress demand to capacity ratios q/q_c of the soil-foundation system were proposed as:

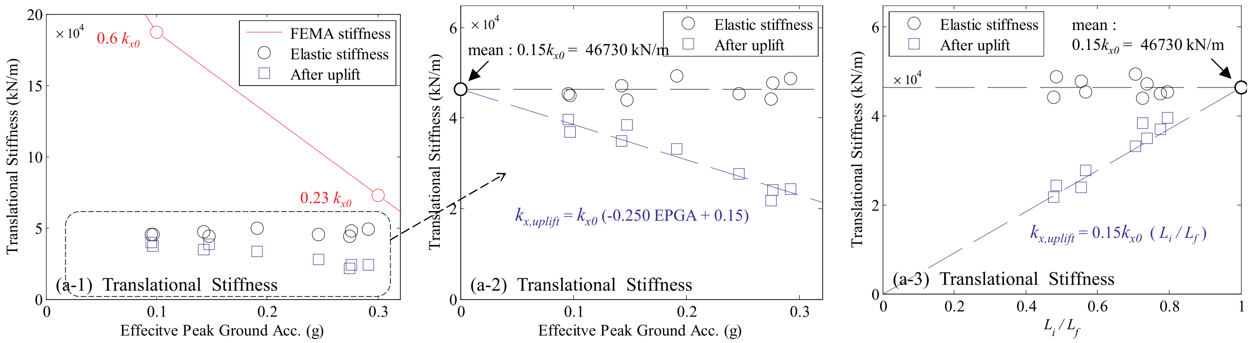

(a) Translational stiffness

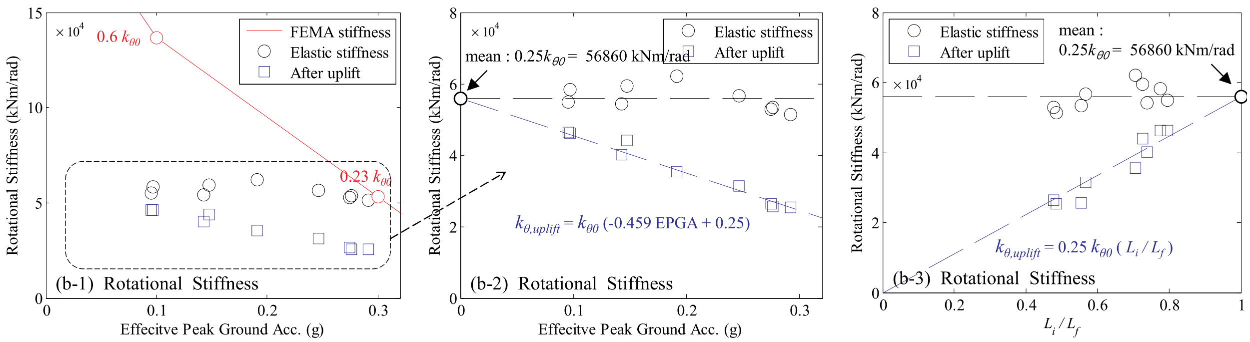

(b) Rotational stiffness

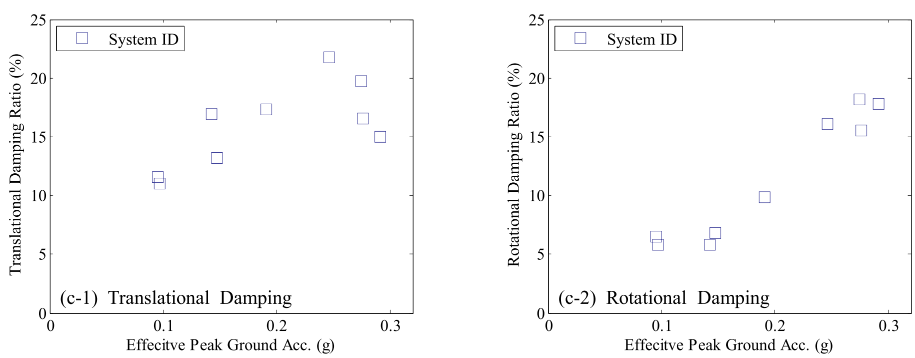

(c) Damping ratio

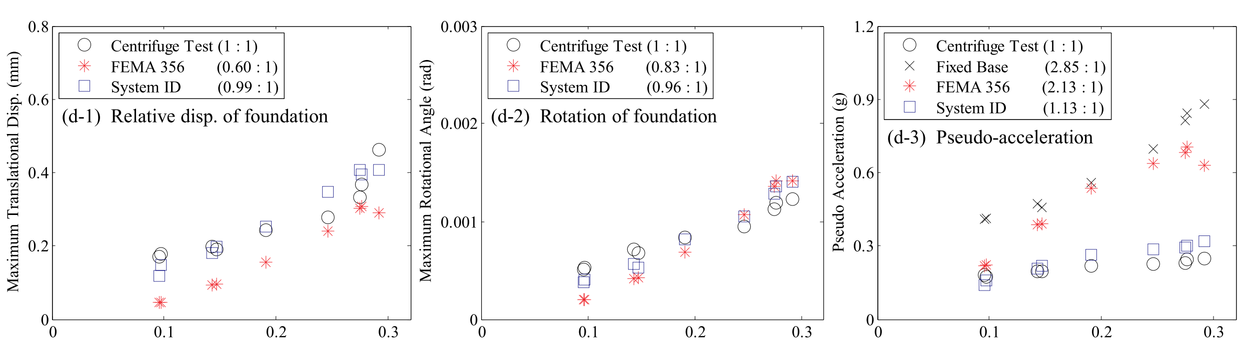

(d) Maximum responses for both the foundation and the SDOF-4

Fig. 10. System identification results for SDOF-4.

Table 4
Variations of inelastic stiffness, according to EPGA and L_i / L_f.

stiffness	q/q_c	Initial elastic stiffness before uplift	Stiffness after uplift
Translation	0.016	$k_x = 0.12\,k_{x0}$	$k_x = k_{x0}(0.12 - 0.276\,EPGA)$ $k_x = 0.12\,k_{x0} \times (L_i/L_f)$
	0.021	$k_x = 0.15\,k_{x0}$	$k_x = k_{x0}(0.15 - 0.250\,EPGA)$ $k_x = 0.15\,k_{x0} \times (L_i/L_f)$
Rotation	0.016	$k_\theta = 0.19\,k_{\theta0}$	$k_\theta = k_{\theta0}(0.19 - 0.396\,EPGA)$ $k_\theta = 0.19\,k_{\theta0} \times (L_i/L_f)$
	0.021	$k_\theta = 0.25\,k_{\theta0}$	$k_\theta = k_{\theta0}(0.25 - 0.459\,EPGA)$ $k_\theta = 0.25\,k_{\theta0} \times (L_i/L_f)$

$$k_x = 7.5\ k_{x0}\ q/q_c\ \le\ k_{x0} \tag{53}$$

$$k_\theta = 12\ k_{\theta0}\ q/q_c\ \le\ k_{\theta0}. \tag{54}$$

4.4. Stiffness degradation after uplift

As the EPGA increased, the stiffness after uplift decreased linearly from the elastic stiffness, as shown in Figs. 9(a-2), Fig. 9(b-2), Fig. 10(a-2), and Figs. 10(b-2) (blue-square markers). This indicates that the reduction of contact area and the increase of earthquake intensity reduced the stiffness of shallow foundation. In this study, linear functions for the stiffness after uplift derived from regression analyses are summarized in Table 4. Also, Figs. 9(a-3), Fig. 9(b-3), Figs. 10(a-3), and Figs. 10(b-3) show linear relationships between the stiffness and the contact area L_i, which was calculated from the measured accelerations using Eq. (1) and the vertical equilibrium.

4.5. Damping increase after uplift

In Figs. 9(c-1), Fig. 9(c-2), Figs. 10(c-1), and Figs. 10(c-2), damping ratios according to the EPGA scenario are presented. As the EPGA increased, damping ratios also increased up to 20%, due to mobilization of the contact area between the foundation and sub-soil.

4.6. Maximum responses of foundation and structure

The maximum responses for both foundations and structures (calculated using estimated dynamic properties and FEMA 356) were then compared to centrifuge test results shown in Figs. 9(d) and Fig. 10(d). Ratios in the figure legends indicate the average ratios of the calculated responses to the test results. As FEMA 356 overestimated stiffness, the maximum relative displacements and rotations of the foundation were 22–83% those of the test results. Alternatively, the maximum relative displacement and rotation of the foundation estimated by the SI were close to the test results, with accuracy values that varied between 88% and 99%. As per the stiffness and damping ratios, pseudo-accelerations (calculated by Eq. (55) using the net displacements of the structures), were close to the test results, with accuracies that varied from 102% to 113%, as shown in Figs. 9(d-3) and Fig. 10(d-3).

$$S_a = \frac{k_s \cdot u_{Net}}{m_s} \tag{55}$$

Pseudo-accelerations calculated from fixed base models were 38% and 185% greater than the test results. The pseudo-accelerations of the structures calculated by FEMA 356 were also 32% and 213% greater than the test results, and were close to those of fixed base models.

4.7. Limitations of this study

In this study, the uncoupled model was used to identify the rocking foundation. However, the translational and rotational responses of foundation were coupled by the medium of contact area from the centrifuge tests by Kim et al. [10]; Thus, the contact area should be considered in the system identification model as a future study. Even though the uncoupled model was used in this study, the system identification results show the coupled nonlinear behavior between translation and rotation of foundation.

The proposed relationships improved the stiffness of FEMA 356 by considering the q/q_c ratio. However, these relationships were based on the previous centrifuge test [10]; in this study, the soil was not as stiff as in the S_E site class, and thus the q/q_c was very small (0.016 and 0.021). Therefore, our relationship is probably particular to our test soil conditions, specifically small q/q_c values and S_E site class. To generalize this proposed relationship, system identification should be performed using many test variables, including various soil and foundation conditions.

5. Conclusions

In this study, we applied system identification using the Extended Kalman Filter to a soil-foundation-structure system. We used centrifuge tests to determine simultaneously nonlinear translational, rotational stiffness, and damping coefficients in the time domain, and compared these values to those obtained using FEMA 356.We used an S_E site class, and a bearing stress demand to capacity ratio (q/q_c) that ranged from 0.016 and 0.021. The structure periods were 0.26 s for SDOF-3 and 0.36 s for SDOF-4, and the results are summarized as follows.

1) When the q/q_c was 0.016, the elastic translational stiffness was 12% of the translational stiffness, and the mean elastic rotational stiffness was19% of the rotational stiffness (according to FEMA 356). As the q/q_c increased to 0.021, the mean elastic translational stiffness was 15% of the translational stiffness, and the mean elastic rotational stiffness was 25% of the rotational stiffness (according to FEMA 356).
2) After partial uplift occurred in the foundation, the translational and rotational stiffness rapidly decreased in the time domain due to a decrease in contact area between the foundation and sub-soil. The stiffness at the maximum response reduced linearly, according to the effective peak ground acceleration (EPGA).
3) After partial uplift, damping coefficients rapidly increased in the time domain, due to mobilization of the contact area between the foundation and sub-soil. As the EPGA increased, the damping ratios increased up to 20%.
4) FEMA 356 overestimated the foundation stiffness for the S_E site class. Thus, the dynamic response of the foundation (calculated using the FEMA 356 stiffness) was smaller than that found using centrifuge tests.
5) On the basis of the system identification results, a relationship between the elastic stiffness and the q/q_c ratio was proposed for small q/q_c and S_E site classes.

Acknowledgement

This work was supported by the National Research Foundation of Korea, Project no. NRF- 2019R1A6A1A07025819 and by the Ministry of Land, Infrastructure, and Transport Affairs of the Korean Government (Grant no. 14-RERP-B082884-01 from the Housing Environmental Research Project).

References

[1] Housner GW. The behavior of inverted pendulum structures during earthquakes. Bull Seismol Soc Am 1963;53(2):403–17.
[2] Antonellis G, Gavras A, Panagiotou M, Kutter B, Guerrini G, Sander A, Fox P. Shake table test of large-scale bridge columns supported on rocking shallow foundations. J Geotech Geoenviron Eng ASCE 2015;10:04015009. 1061/(ASCE)GT.1943-5606.0001284.

[3] Madaschi A, Gajo A, Molinari M, Zonta D. Characterization of the dynamic behavior of shallow foundations with full-scale dynamic tests. J Geotech Geoenviron Eng ASCE 2016;10:04016026. 1061/(ASCE)GT.1943-5606.0001446.
[4] Wittich CE, Hutchinson TC. Shake table tests of stiff, unattached, asymmetric structures. Earthq Eng Struct Dyn 2015;44(14):2425–43.
[5] Drosos V, Georgarakos T, Loli M, Anastasopoulos I, Zarzouras O, Gazetas G. Soil-foundation-structure interaction with mobilization of bearing capacity: experimental study on sand. J Geotech Geoenviron Eng ASCE 2012;138(11):1369–86.
[6] Anastasopoulos I, Drosos V, Antonaki N. Three-storey building retrofit: rocking isolation versus conventional design. Earthq Eng Struct Dyn 2015;44(8):1235–54.
[7] Loli M, Knappett JA, Brown MJ. Centrifuge modeling of rocking-isolated inelastic RC bridge piers. Earthq Eng Struct Dyn 2014;43(15):2341–59.
[8] Liu W, Hutchinson T, Gavras A, Kutter B, Hakhamaneshi M. Seismic behavior of frame-wall-rocking foundation systems. I: test program and slow cyclic results. J Struct Eng ASCE 2015;10. 1061/(ASCE)ST.1943-541X.0001264, 04015059.
[9] Trombetta N, Mason H, Hutchinson T, Zupan J, Bray J, Kutter B. Nonlinear soil–-foundation–structure and structure–soil–structure interaction: centrifuge test observations. J Geotech Geoenviron Eng ASCE 2013;10:04013057. 1061/(ASCE)GT.1943-5606.0001074.
[10] Kim D, Lee S, Kim D, Choo Y, Park H. Rocking effect of a mat foundation on the earthquake response of structures. J Geotech Geoenviron Eng ASCE 2015;10:04014085. 1061/(ASCE)GT.1943-5606.0001207.
[11] Antonellis G, Panagiotou M. Seismic response of bridges with rocking foundations compared to fixed-base bridges at a near-fault site. J Bridge Eng ASCE 2014;10:04014007. 1061/(ASCE)BE.1943-5592.0000570.
[12] Anastasopoulos I, Kontoroupi Th. Simplified approximate method for analysis of rocking systems accounting for soil inelasticity and foundation uplifting. Soil Dyn Earthq Eng 2014;56:28–43.
[13] Chen S, Shi J. A simplified model for coupled horizontal and rocking vibrations of embedded foundations. Soil Dyn Earthq Eng 2013;48:209–19.
[14] Lu Y, Marshall AM, Hajirasouliha I. A simplified nonlinear sway-rocking model for evaluation of seismic response of structures on shallow foundations. Soil Dyn Earthq Eng 2016;81:14–26.
[15] Gajan S, Kutter B. Contact interface model for shallow foundations subjected to combined cyclic loading. J Geotech Geoenviron Eng ASCE 2009;135(3):407–19.
[16] Allmond J, Kutter B. Design considerations for rocking foundations on unattached piles. J Geotech Geoenviron Eng ASCE 2014;10:04014058. 1061/(ASCE)GT.1943-5606.0001162.
[17] Deng L, Kutter B, Kunnath S. Seismic design of rocking shallow foundations: displacement-based methodology. J Bridge Eng ASCE 2014;10:04014043. 1061/(ASCE)BE.1943-5592.0000616.
[18] Gazetas G, Anastasopoulos I, Garini E. Geotechnical design with apparent seismic safety factors well-bellow 1. Soil Dyn Earthq Eng 2014;57:37–45.
[19] Gazetas G. Formulas and charts for impedances of surface and embedded foundations. J Geotech Eng ASCE 1991;117(9):1363–81.
[20] Deng L, Kutter B, Kunnath S. Centrifuge modeling of bridge systems designed for rocking foundations. J Geotech Geoenviron Eng ASCE 2012;138(3):335–44.
[21] Oskay C, Zeghal M. A survey of geotechnical system identification techniques. Soil Dyn Earthq Eng 2011;31(4):568–82.
[22] Tileylioglu S, Stewart J, Nigbor R. Dynamic stiffness and damping of a shallow foundation from forced vibration of a field test structure. J Geotech Geoenviron Eng ASCE 2011:344–53. 10.1061/(ASCE)GT.1943-5606.0000430.
[23] Safak E. Time-domatin representation of frequency-dependent foundation impedance function. Soil Dyn Earthq Eng 2006;26(1):65–70.
[24] Snieder R, Safak E. Extracting the building response using seismic interferometry: theory and application to the Millika library in Pasadena, California. Bull Seismol Soc Am 2006;96(2):586–98.
[25] Ghahari SF, Ghannad MA, Taciroglu E. Blind identification of soil-structure systems. Soil Dyn Earthq Eng 2013;45(1):56–69.
[26] FEMA. NEHRP commentary on the seismic rehabilitation of buildings vol. 274. Washington DC: FEMA; 1997.
[27] FEMA. Prestandard and commentary for the seismic rehabilitation of buildings vol. 356. Washington, DC: FEMA; 2000.
[28] Terejanu G. Extended Kalman filter tutorial. Department of Computer Science and Engineering, University at Buffalo; 2008. [Web-tutorial].
[29] Kim SP. Essential Kalman filter. Korea: A-Jin; 2008.
[30] Mikami A, Sawada T. Time-domain identification system of dynamic soil-structure interaction. 13th world conference on earthquake engineering, Vancouver, Canada. 2004. Paper No. 747.
[31] ATC. Tentative provisions for the development of seismic regulations for buildings, ATC-3-06 report. Redwood City, CA: Applied Technology Council; 1978.